ORIGINAL ARTICLE

Neurons with Multiple Axons Have Functional Axon Initial Segments

Yu Guo[1] · Zhuo Liu[1,2] · Yi-kun Chen[1] · Zhen Chai[1] · Chen Zhou[1] ·
Yan Zhang[1]

Abstract Neurons grow multiple axons after treatment with glycogen synthase kinase-3 (GSK-3) inhibitors. However, whether they are electrically active is not known. Here, we examined the role of multiple axons as electrophysiological components during neuronal firing. Combining pharmacological, immunofluorescence, and electrophysiological methods, we found that more neurons had multiple axon initial segments (AISs) after inhibition of GSK-3 activity with SB415286. The multiple AISs induced by GSK-3 inhibition were enriched with voltage-gated sodium channels. The depolarization rate of the multiple-AIS neurons was increased, but their action potential threshold and half-width were normal. By calculating derivatives of the action-potential rising phase, an extra $\mathrm{d}^2V/\mathrm{d}t^2$ peak from the extra AIS was distinguished; this indicated that the extra AIS fired ahead of the soma and increased the rate of depolarization. Our study demonstrates that the multiple axons induced by GSK-3 inhibition have AIS structures that are electrically active, and provides insight for axon and AIS studies.

Keywords Axon initial segment · Axon · GSK-3 · Ankyrin G · Electrophysiology · Immunofluorescence

Yu Guo and Zhuo Liu have contributed equally to this work.

✉ Chen Zhou
akiba@pku.edu.cn

✉ Yan Zhang
yanzhang@pku.edu.cn

[1] State Key Laboratory of Membrane Biology, College of Life Sciences, Peking University, PKU-IDG/McGovern Institute for Brain Research, Beijing 100871, China

[2] Department of Forensic Science, People's Public Security University of China, Beijing 100038, China

Introduction

Neurons are polarized cells with two distinct structural compartments: multiple dendrites and a single axon. During development, the appearance of axons initiates the compartmentalization of neurons and polarized transportation of materials. Other important functions of axons include firing and conducting action potentials, which play a vital role in neuronal network activity [1]. Several studies have focused on the establishment and maintenance of neuronal polarity [2, 3], which are regulated by many factors. Glycogen synthase kinase-3β (GSK-3β) and its upstream regulators, such as Akt (also called protein kinase B) and phosphatase and tensin homolog (PTEN), modulate other molecules critical for specifying axon fate [4, 5]. These factors act on the neuronal cytoskeletal system to alter microtubule stability, which is the initial event in neuronal polarization [6]. Soon, a diffusion barrier arises at the initial segment of the axon, which contributes to polarized protein delivery between axons and soma-dendrites [7, 8]. This specialized region, the axon initial segment (AIS), has attracted much attention in recent years.

The AIS is generally a thin, unmyelinated region of a proximal axon (10–60 μm in length) [9] that plays a critical role in the maintenance of neuronal polarity and action potential initiation [9–11]. As a molecular barrier, numerous cytoskeletal and cell adhesion molecules assemble at the AIS to control material transportation into the axon and maintain its unique molecular composition [8, 12]. As the site of action potential initiation, the AIS is characterized by its enrichment in ion channels, especially voltage-gated sodium channels (Nav channels) [13]. The functions of the AIS rely on an adaptor protein ankyrin G (AnkG), which is responsible for recruiting many other AIS proteins [14–16]. Therefore, the AIS can be identified by labeling AnkG,

642

Neurosci. Bull. December, 2017, 33(6):641–652

Nav channels, neurofascin, and other AIS proteins [17–19]. The AIS is disrupted in pathological conditions such as Alzheimer's disease and ischemia [20, 21]. Although remodeling of the AIS has been described in a study of the peri-infarct areas of mice with ischemia [22], functional recovery was not reported.

Recently, changes in cytoskeletal stabilization in polarized neurons have been found to induce the formation of multiple axons from pre-existing dendrites. And drugs that depolymerize actin or inhibit GSK-3β activity have been found to induce the formation of multiple axons, which are capable of vesicle recycling [4, 23]. However, these studies did not show whether the multiple axons induced by pharmacological treatments are electrophysiologically active or affect the firing properties of a neuron. In this study, we used SB415286 (SB41), a GSK-3 inhibitor, to induce multiple axons in cultured hippocampal neurons and studied the electrophysiological characteristics of the extra axons and their potential to interfere with normal neuronal functions.

Materials and Methods

Primary Hippocampal Neuron Culture

Primary neurons were cultured from newborn Sprague-Dawley rat hippocampus. All the animal experimental protocols were approved by the Institutional Animal Care and Use Committee of Peking University [20]. Briefly, fresh hippocampal tissue samples were dissected in Hanks' balanced salt solution (HBSS) (Life Technologies, Thermo Fisher Scientific, Shanghai, China) and digested (20 min, 37 °C) with 0.25% trypsin (Solarbio, Beijing, China), then inactivated by 10% decomplemented fetal bovine serum (FBS) (Life Technologies). The mixture was gently triturated through a pipette to produce a homogenous mixture. The undispersed pieces were allowed to settle for 1 min, after which the supernatant was centrifuged. The pellet containing cells was dispersed and re-suspended in Dulbecco's modified Eagle's medium (DMEM)/F-12 containing $1\times$ penicillin-streptomycin with 10% FBS (all from Life Technologies). Neurons were plated on poly-D-lysine-coated (0.1 g/mL, Sigma-Aldrich) glass coverslips at 1×10^5 cells/mL. Neurons were incubated at 37 °C (5% CO_2) in DMEM/F-12 containing penicillin-streptomycin (100 µg/mL) with 10% FBS. Four hours after plating, the medium was replaced with Neurobasal medium plus B27 supplement (2%) with additional glutamax (500 µmol/L) (all from Life Technologies) and penicillin-streptomycin (100 µg/mL). Half of the medium was replaced every 72 h. After plating, hippocampal neurons were treated with SB41 (Tocris, Bristol, UK) or vehicle (dimethyl sulfoxide, DMSO) and cultured for 7 days.

Immunostaining and Imaging

As described previously [20], the cultures were fixed with 4% paraformaldehyde (for AnkG and neurofascin labeling) or 0.5% paraformaldehyde containing 0.5% sucrose (for pan-Nav labeling) at room temperature (RT) for 20 min and permeabilized in PBS-Triton at 4 °C for 15 min. The cultures were blocked with 5% bovine serum albumin (BSA) at RT for 1 h, followed by incubation overnight at 4 °C with primary antibodies: mouse monoclonal anti-AnkG (Life Technologies, 1:500), mouse monoclonal anti-pan-Nav (Sigma, 1:1000), chicken polyclonal anti-microtubule-associated protein 2 (MAP2; Abcam, 1:10000), or rabbit polyclonal anti-neurofascin (Abcam, 1:1000). Alexa Fluor anti-mouse 568, anti-chicken 633 and anti-rabbit 488 (Life Technologies, 1:500; 1 h at RT) were applied as secondary antibodies. Nuclei were stained with DAPI (4′,6-diamidino-2-phenylindole, 1 µg/mL; Life Technologies) at RT for 15 min in the dark. Finally, coverslips were mounted onto glass slides containing the samples using Immunon mounting medium (SouthernBiotech, Birmingham, AL).

Images were acquired with a laser confocal fluorescence microscope (Zeiss LSM 710 NLO, Oberkochen, Germany) with appropriate excitation and emission filters under a $40\times$ water lens. Analysis was performed using ZEN2009 (Zeiss, Oberkochen, Germany) or ImageJ software (National Institutes of Health, Bethesda, MD). To measure the position of AnkG, we drew a line profile starting at the soma and extending through and past the AIS. The raw data on this line were processed with a program written in IDL 8.0 (Interactive Data Language 8.0, Harris Geospatial Solutions, Broomfield, CO). Fluorescence intensity values were measured at each pixel (1 pixel = 0.297 µm) along this profile. The profiles were smoothed using a 8-point ($\sim$5 µm) sliding mean and normalized between 1 (maximum smoothed fluorescence, location of the AIS max position) and 0 (minimum smoothed fluorescence). The start and end positions of the AIS were obtained at the proximal and distal axonal positions, where the normalized and smoothed profile declined to 0.3 [19]. We used ImageJ to measure the fluorescence intensity of pan-Nav in the AIS and soma. The polygon tool was used to outline the AIS and soma area. The mean and total fluorescence intensity in the area were output by ImageJ. For each multiple-axon neuron measured, single-axon neurons in the same field were selected as controls.

Live Labeling of the AIS

As previously described [21], mouse monoclonal antibodies (A12/18; NeuroMab) that recognize an extracellular epitope of neurofascin were used for live labeling of the

AIS. Conditioned medium was removed from hippocampal neuron cultures at DIV (days *in vitro*) 8–9 and stored for later use. Next, the cells were gently washed twice in HBSS and incubated with the primary antibody anti-neurofascin (1:200, 30 min, 37 °C) diluted in fresh medium, followed by 3 washes in HBSS and incubation with Alexa Fluor anti-mouse 568 secondary antibody (1:500; 30 min, 37 °C). After a final wash in HBSS, nuclei were stained with Hoechst 33342 diluted in fresh medium (5 μg/mL; Life Technologies) at 37 °C in the dark for 20 min. The Hoechst stain was removed, then fresh and conditioned medium was added to the cells at a 1:1 ratio.

Electrophysiology

Hippocampal neurons were used for whole-cell patch clamp recording at DIV 8–9. Patch pipettes (3–6 MΩ) were pulled with a P-97 Micropipette Puller (Sutter Instrument, Novato, CA) and filled with internal solution (in mmol/L: K-gluconate 130, NaCl 10, MgCl$_2$ 1, HEPES 10, EGTA 10, ATP-Mg 4, phosphocreatine-Tris 10, GTP-Li 0.3; pH adjusted to 7.2–7.3 with KOH). Each test neuron was submerged in artificial cerebrospinal fluid (in mmol/L: NaCl 141, KCl 2.5, CaCl$_2$ 2.4, MgCl$_2$ 1.3, NaH$_2$PO$_4$ 1.25, glucose 10, HEPES 10; pH adjusted to 7.3–7.4 with NaOH). Live cell imaging was acquired using Xcellence software (Olympus, Tokyo, Japan). Patch recordings were obtained using a HEKA EPC-10 (HEKA, Lambrecht, Germany) amplifier at RT. Signals were digitized at 100 kHz. When action potentials were triggered, the membrane potential was held at −70 mV under current-clamp mode, after which a step current of 5 pA was injected until the just-suprathreshold current was reached. This current was injected for 200 ms at 1-s intervals to trigger action potentials. When sodium and potassium currents were recorded, the cell membrane potential was held at −80 mV under voltage-clamp mode and step-depolarized (5 mV/step) to 70 mV. Action potential properties and currents were measured using Clampfit 10.0 (Molecular Devices, Sunnyvale, CA). The first and second derivatives (dV/dt and d^2V/dt^2) of the action potential waveforms, and the peak value of d^2V/dt^2 were calculated with programs written in IDL (Interactive Data Language, Harris Geospatial Solutions, Broomfield, CO).

Statistics

SigmaPlot 10.0 and SigmaStat 3.5 (Systat Software Inc., San Jose, CA) were used to analyze the electrophysiological data. Other data analysis were performed using Graphpad Prism (GraphPad Software, La Jolla, CA). Results are reported as mean ± SEM. Student's *t*-test (unpaired) or two-way ANOVA was used to determine the significance of differences between sets of 2 or multiple independent samples. Pearson correlation was used in the correlation analysis. All tests were two-tailed. The threshold for significance was 0.05.

Results

Multiple Axons Induced by Pharmacological Inhibition of GSK-3 Have AISs

We used SB41, a pharmacological inhibitor of GSK-3, to induce multiple axons in primary hippocampal neuron cultures [4]. By using anti-AnkG antibodies to label AISs, we found that SB41 significantly decreased the number of neurons with a single AIS, but increased the number of neurons with multiple AISs (Fig. 1A). There was a significant difference ($t_8 = 4.769$, $P < 0.01$) in the multiple-AIS neuron ratio between the SB41 (38.14% ± 3.79%) and DMSO control (17.10% ± 2.25%) groups (Fig. 1B). Here, the ratio was close to that of multiple-axon neurons induced by a GSK-3 inhibitor reported in a previous study, in which such neurons were indicated by Tau-1 [4], revealing that these supernumerary axons had AISs. To confirm these results, we used antibodies against the cell-adhesion molecule neurofascin, another protein located in the AIS region. As expected, SB41 treatment significantly increased the number of neurons with multiple AISs (47.97% ± 2.239%) (Fig. 1C). Our results demonstrated that supernumerary axons induced by GSK-3 inhibition have AIS structures.

To determine whether the distribution of AnkG on each AIS was changed in multiple-axon neurons, the position and fluorescence intensity of AnkG were measured (Fig. 1D). The AISs of multiple-axon neurons were closer to the soma both in groups treated with DMSO and with SB41 (Fig. 1E), indicating a proximal shift of the AIS. At the same time, the length of an AIS was shorter in multiple-axon neurons (Fig. 1F). SB41 also shortened the AIS in single-axon neurons compared to those treated with DMSO (Fig. 1F). In addition, the average fluorescence intensity of AnkG was lower in multiple-axon neurons (Fig. 1G). No difference was detected in the somatic AnkG level between single- and multiple-axon neurons, although SB41 increased the somatic AnkG level (Fig. 1H). These results demonstrated that the morphology of AIS is changed in multiple-axon neurons due to alterations in AnkG distribution. Considering the critical role of the AIS in action potential initiation, the change in somatic AnkG was not considered in subsequent experiments. Since SB41 treatment caused similar structural changes of the AIS in single- and multiple-axon neurons compared to DMSO treatment, the effect of multiple axons was examined in SB41-treated neurons in the following experiments.
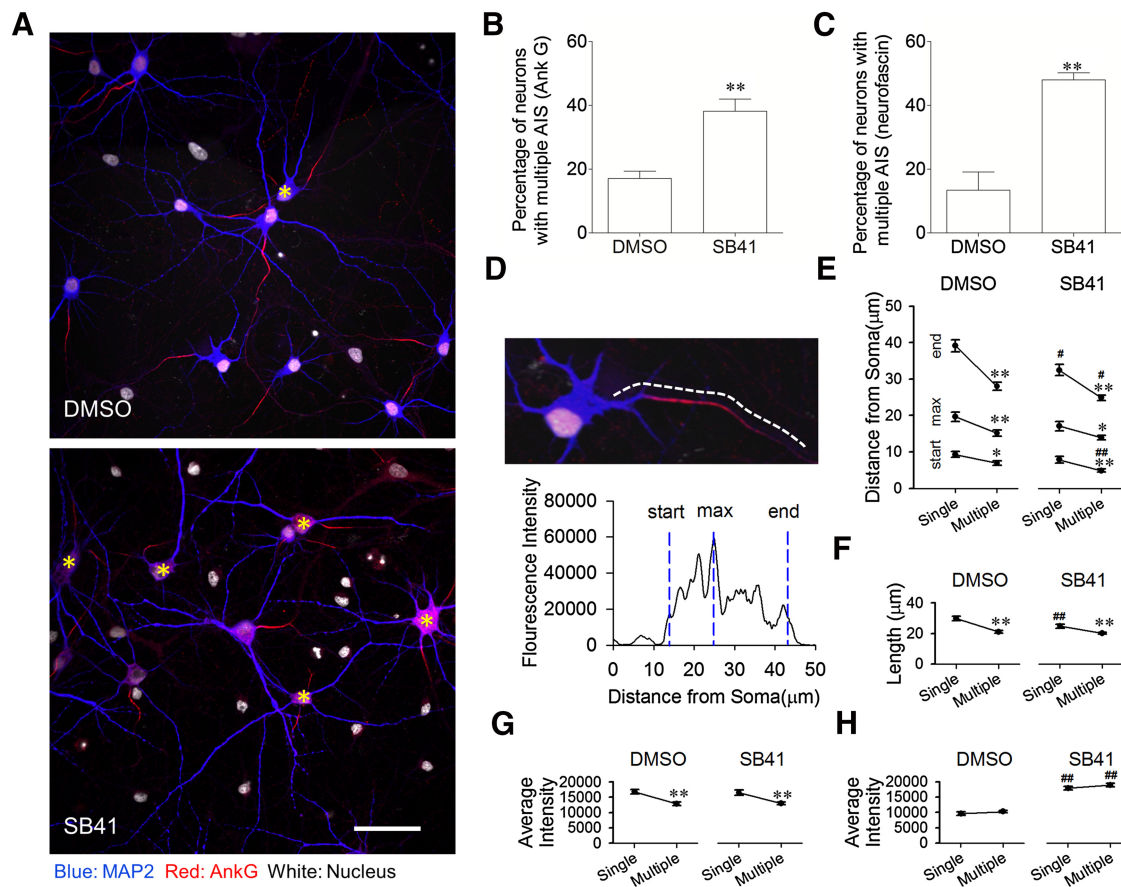
Blue: MAP2 Red: AnkG White: Nucleus

Fig. 1 Multiple axons induced by pharmacological inhibition of GSK-3 activity in cultured primary hippocampal neurons have axon initial segments (AISs) and different AnkG distribution. **A** Representative images of neurons treated with DMSO (*upper panel*) or SB41 (*lower panel*) (scale bar, 50 µm). AISs were identified by AnkG antibodies (*red*), dendrites were identified by MAP2 antibodies (*blue*), and nuclei were stained by DAPI (*white*). Asterisks indicate neurons with multiple AISs. **B, C** Proportions of neurons with multiple AISs as indicated by AnkG (**B**, $t_8 = 4.769$, $P = 0.0014$) or neurofascin (**C**, $t_4 = 5.253$, $P = 0.0063$) antibodies in both groups (data from 3 (neurofascin) or 5 (AnkG) independent repeated experiments;

$P < 0.01$, t-test). **D *Upper panel*, representative image showing the measurement of AnkG on an AIS. The *dashed line* indicates the position of the AIS. *Lower panel*, the change of AnkG fluorescence intensity on an AIS along with distance. **E** Multiple-axon neurons had AISs closer to the soma. **F** The average length of AIS was shorter in multiple-axon neurons. **G** The fluorescence intensity of AnkG on each AIS was decreased in multiple-axon neurons. **H** The somatic AnkG level did not differ between single- and multiple-axon neurons. n = DMSO single 45, multiple 45; SB41 single 73, multiple 85 AIS, from 2 experiments; **$P < 0.01$ in DMSO or SB41 groups, ##$P < 0.01$ in single or multiple groups, two-way ANOVA.

Distribution of Nav Channels on the AISs of Multiple Axons Differs from That of a Single Axon

To perform its normal function, the AIS is enriched with many other proteins such as Nav channels and neurofascin [11, 13, 24]. Thus, we used pan-Nav antibodies to characterize the Nav channel distribution on each AIS of multiple-axon neurons after SB41 treatment (Fig. 2A). All AISs on multiple-axon neurons showed neurofascin and Nav channel staining, which co-localized well with AnkG. As previous studies have revealed that the position and length of AISs are associated with neuronal excitability [25], we measured the distribution of Nav channels on axons and soma. The Nav channels of the multiple-axon neurons were distributed closer to the

soma than those of the single-axon neurons (Fig. 2B). This relocation of the AIS was accompanied by a change in the Nav signal length, which was shorter in the multiple-axon neurons (Fig. 2C). Compared with single-axon neurons, the fluorescence intensity and density of Nav channels at each AIS region were lower in multiple-AIS neurons (Fig. 2D, E). However, there was no difference in the total AIS Nav channel fluorescence between single- and multiple-axon neurons (Fig. 2F). Analysis of the average fluorescence intensity of somatic Nav channels (Fig. 2G, H) and total Nav channels on neurons (Fig. 2I) revealed no difference between the two groups. These results suggest that neurons with different numbers of AISs may have different electrophysiological properties.
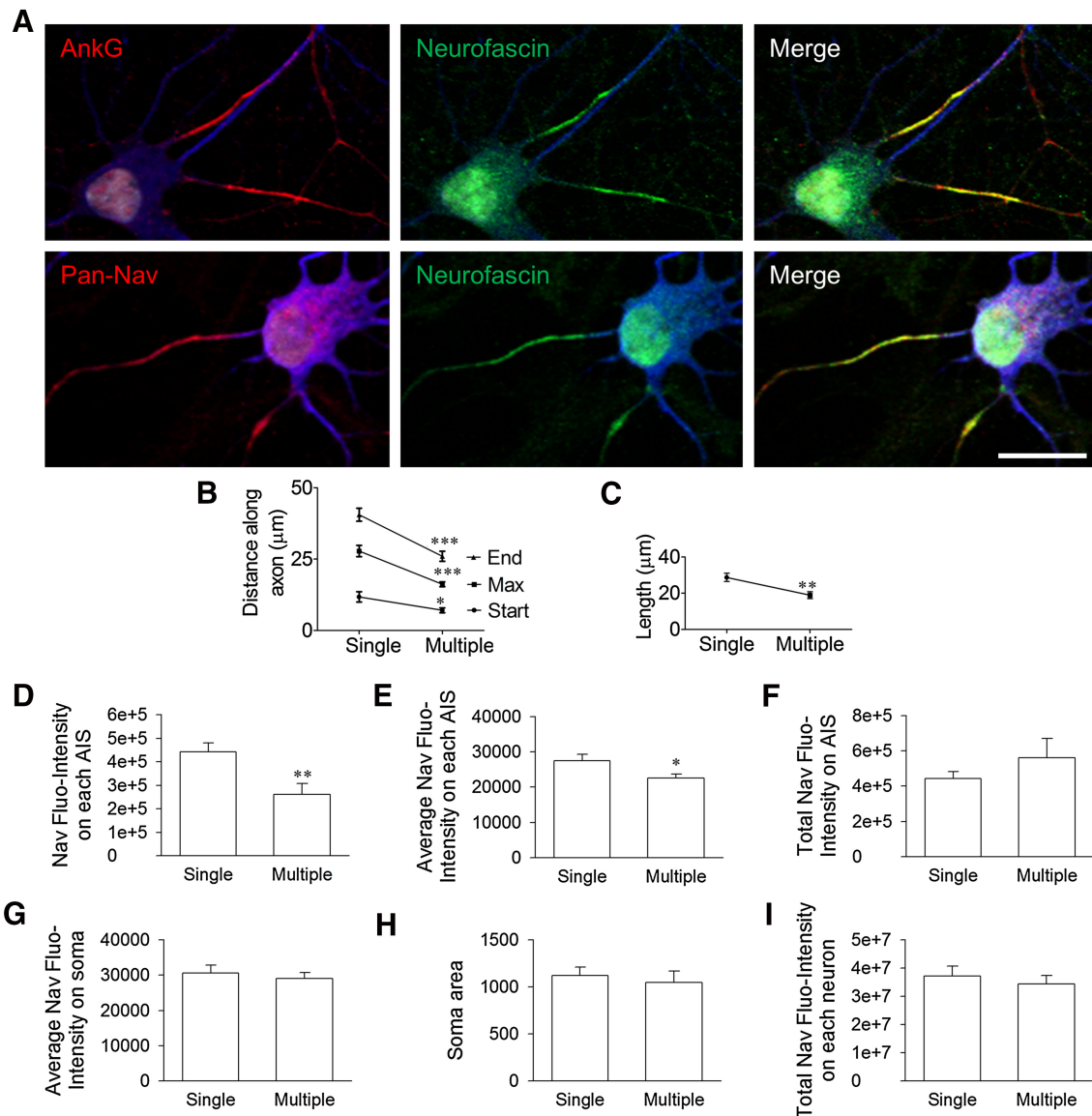
Fig. 2 Changes in Nav channel distribution on AISs of multiple-axon neurons. **A** Representative images of multiple-axon neurons with AnkG and neurofascin staining (*upper panel*), or with Nav channel and neurofascin staining (*lower panel*) (scale bar, 20 μm). **B** Positions of the start ($t_{79} = 2.421$, $P = 0.0178$), maximum (max) ($t_{79} = 5.591$, $P < 0.0001$), and end ($t_{79} = 5.088$, $P < 0.0001$) of AISs (multiple, $n = 42$ AISs from 21 neurons; single, $n = 39$ AIS from 39 neurons). **C** Lengths of AISs (multiple, $n = 42$ AISs; single, $n = 39$ AISs; $t_{79} = 3.379$, $P = 0.0011$, *$P < 0.05$, **$P < 0.01$, ***$P < 0.001$, *t*-test). **D**, **E** Fluorescence intensity (**D**, $t_{46} = 2.738$, $P = 0.0088$) and average fluorescence intensity (**E**, $t_{46} = 2.595$ $P = 0.0127$) of pan-Nav on each AIS and total pan-Nav intensity (**F**, $t_{30} = 1.111$, $P = 0.2753$) on the AIS of each neuron of both groups (multiple, $n = 30$ AISs from 14 neurons; single, $n = 18$ AISs from 18 neurons). **G**, **H**, **I** Average fluorescence intensity of somatic pan-Nav (**G**, $t_{30} = 0.5035$, $P = 0.6183$) and soma area (**H**, $t_{30} = 0.4688$, $P = 0.6426$), as well as the total fluorescence intensity of pan-Nav on each neuron, including the soma and AIS (**I**, $t_{30} = 0.6084$, $P = 0.5475$) (single, $n = 18$; multiple, $n = 14$ neurons).

Single- and Multiple-Axon Neurons Have Similar Whole-Cell Nav Currents and Membrane Properties

Whole-cell voltage-gated sodium (Nav) and potassium (Kv) currents were recorded using patch-clamp. To distinguish neurons with multiple axons from those with a single axon, we labeled the AISs of living neurons with rat monoclonal antibodies recognizing an extracellular epitope of neurofascin before patch-clamp recording (Fig. 3A). Recordings were made from both multiple- and single-axon neurons on the same coverslip. Consistent with the immunofluorescence data, the single- and multiple-axon neurons had similar Nav and Kv currents (Fig. 3C–E). The Nav current tended to be higher in multiple-axon neurons, but the difference was not significant (Fig. 3D). The membrane properties of multiple-axon neurons were
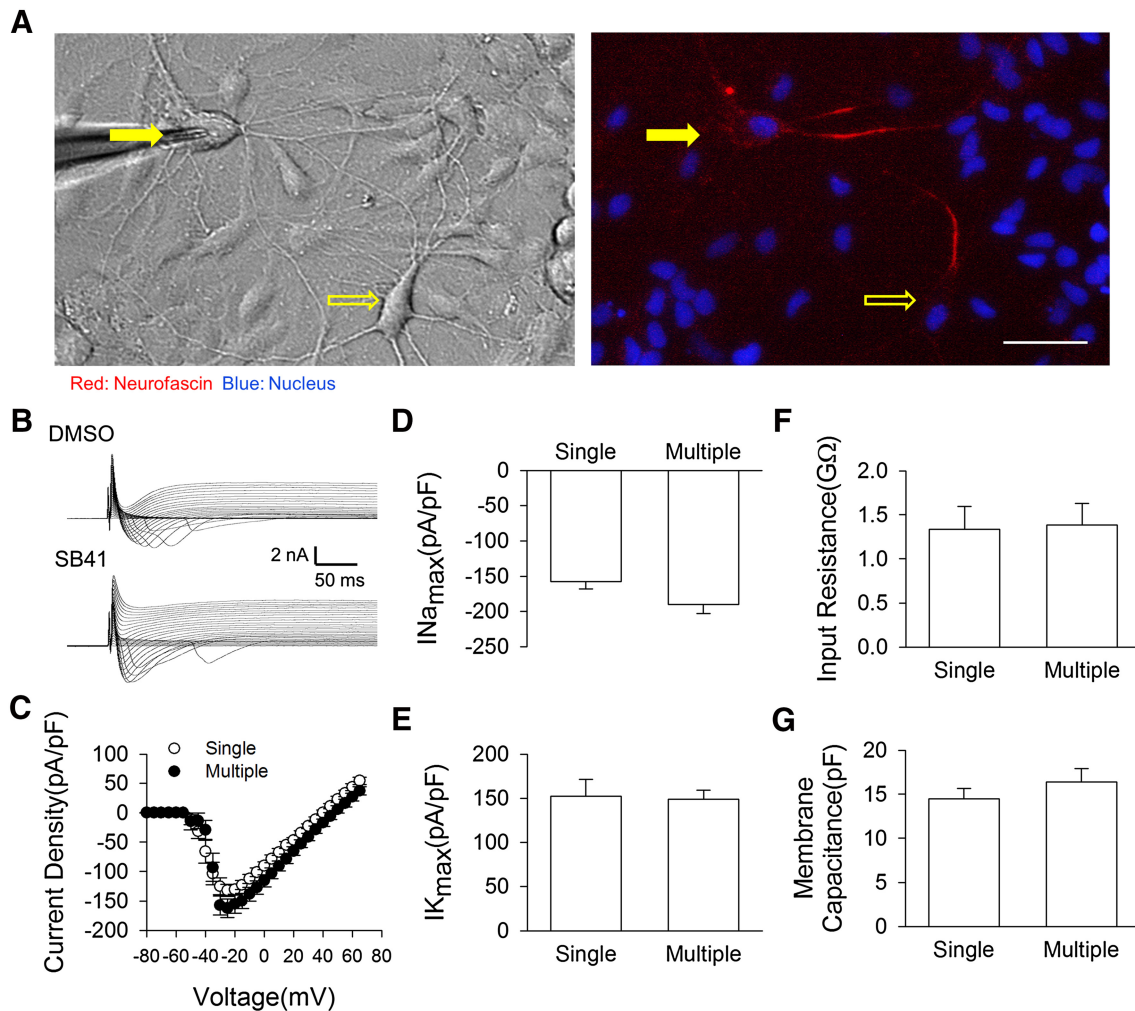
Red: Neurofascin Blue: Nucleus

Fig. 3 Multiple-axon neurons have normal whole-cell Nav current and membrane properties. **A** Live-labeling of AISs with antibodies recognizing an extracellular epitope of neurofascin (*red*); nuclei were stained with Hoechst 33342 (*blue*). Filled arrows, a neuron with two AISs; open arrows, a neuron with one AIS. Scale bar: 50 μm. **B** Typical traces of Nav and Kv currents in DMSO or SB41 treated group, when membrane potentials were depolarized from −80 mV to 70 mV. **C, D** Whole-cell Nav currents were similar in the two groups. **E** Whole-cell Kv currents were unchanged in the multiple-axon neurons. **F, G** There were no differences in input resistance (**F**) or membrane capacitance (**G**). Single, $n = 29$; multiple, $n = 20$ neurons; *t*-test.

similar to those of single-axon neurons, since input resistance and membrane capacitance were not changed (Fig. 3F, G). These results indicate that, rather than increasing the number of Nav channels, induction of multiple AISs only alters their distribution.

## Multiple-Axon Neurons Have Normal Action Potential Threshold

To determine whether the altered Nav channel distribution of the multiple-axon neurons affects their firing properties, we used the whole-cell patch-clamp method to record evoked action potentials (Fig. 4A). The threshold, half-width, and amplitude of action potentials were analyzed (Fig. 4B) and, surprisingly, there was no significant difference between the action potential thresholds of the

multiple-axon and single-axon neurons (Fig. 4C). The action potential half-width of the multiple-axon neurons was slightly shorter than that of the single-axon neurons, but this difference was not significant (Fig. 4D). Consistent with the result for Nav and Kv currents, the overshoot and after-hyperpolarization potential were unchanged in multiple-axon neurons (Fig. 4E, F).

Action Potentials Depolarize Faster in Multiple-Axon Neurons

Although the Nav current and basic action potential properties were unchanged in multiple-axon neurons, the altered distribution of Nav channels might have other effects. Further analysis of action potential waveforms revealed that the depolarizing phase in multiple-axon

Fig. 4 Multiple-axon neurons have normal action potential threshold. **A** An example of triggering action potentials with a just-suprathreshold somatic current injection lasting 200 ms (only the first action potential was used to analyze action potential properties). **B** Typical action potential showing threshold, amplitude, and half-width. **C–F** There were no differences in action potential threshold (**C**), half-width (**D**), overshoot (**E**), or after-hyperpolarization (**F**) (single, $n = 29$; multiple, $n = 20$ neurons; *t*-test).
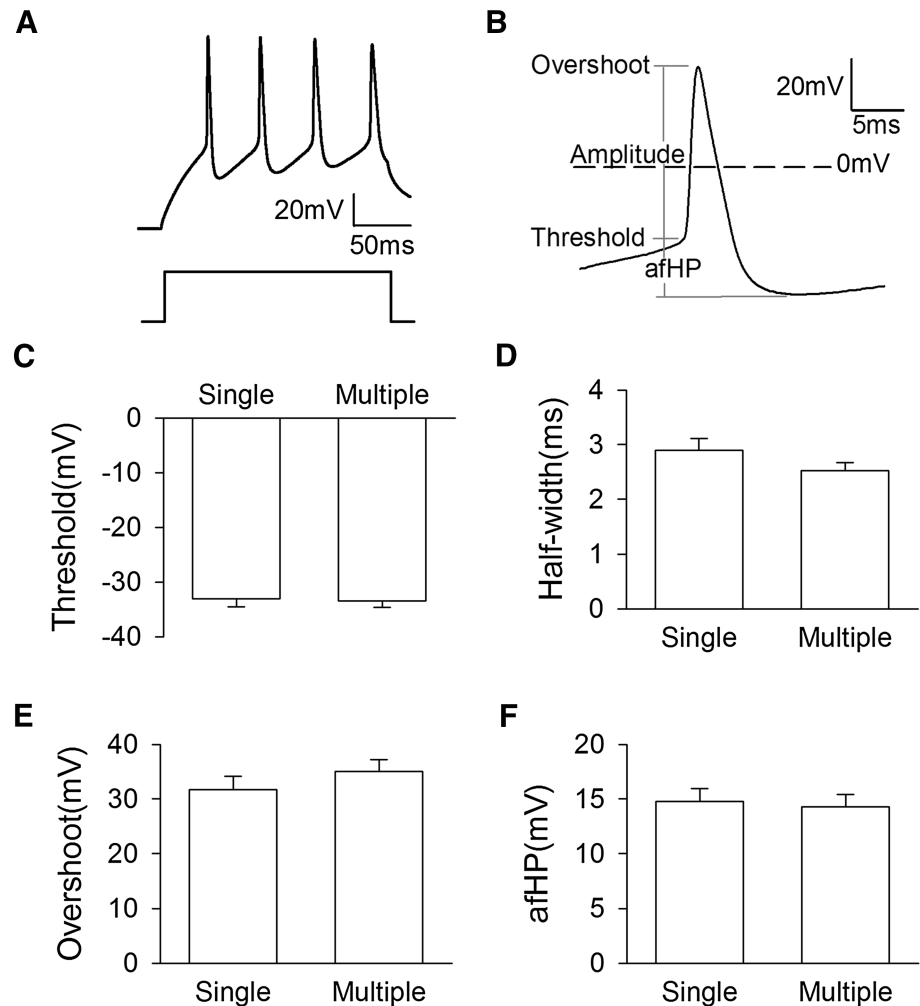
neurons was shorter than that of single-axon neurons (Fig. 5A), and this was associated with a corresponding increase in the rate of depolarization (Fig. 5B). The repolarization phase and repolarization rate of the single- and multiple-axon neurons did not differ significantly (Fig. 5C, D). The depolarizing phase is primarily a result of Nav channel activation, whereas the repolarizing phase is primarily a result of Kv channel activation. Thus, the presence of multiple AISs increased the rate of action potential depolarization, and this change was closely associated with changes in the Nav channel distribution of multiple-axon neurons.

The Faster Depolarization of Multiple-Axon Neurons is Due to Faster Recruitment of Nav Channels

The components of the rising phase can be identified from the time derivative of the action potential (Fig. 6A, B). The first derivative of the action potential (d*V*/d*t*) identified two components: an earlier peak representing the AIS spike, and a later peak representing the somatic spike. The time interval between the two peaks represents the temporal lag between the AIS and the soma due to their impedance mismatch [26, 27]. We compared the first derivatives of the action potential waveforms of single- and multiple-axon neurons (Fig. 6B). Approximately half of the tested single-AIS neurons had two d*V*/d*t* peaks (Fig. 6B upper panel; Fig. 6C, 51.95%), whereas few multiple-axon neurons had two peaks (Fig. 6B lower panel; Fig. 6C, 1.52%). These results suggested that Nav channels may be recruited faster in multiple-axon neurons once depolarization passes the action potential threshold, which reduces the temporal lag between the axonal spike and the somatic spike, fusing them into one peak, and increases the rate of depolarization in multiple-axon neurons (Fig. 5A, B).

To finely dissect the depolarization kinetics of multiple-axon neurons, the second derivative of the action potential (d^2V/dt^2) was calculated; this divided the multiple components and provided reliable information about action potential development (Fig. 6B). Generally, there are two peaks in d^2V/dt^2 waveforms that correspond to two peaks in d*V*/d*t*; in the same way, the first peak is considered to be an

648

Neurosci. Bull. December, 2017, 33(6):641–652

Fig. 5 Multiple-axon neurons depolarize faster than single-AIS neurons during evoked action potentials. **A, B** Multiple-AIS neurons had (**A**) a shorter rising phase and (**B**) higher depolarization rate than single-axon neurons. **C, D** The repolarization phase of multiple-axon neurons did not differ from that of single-axon neurons. (Single, $n = 29$; multiple, $n = 20$ neurons; $*P < 0.05$).
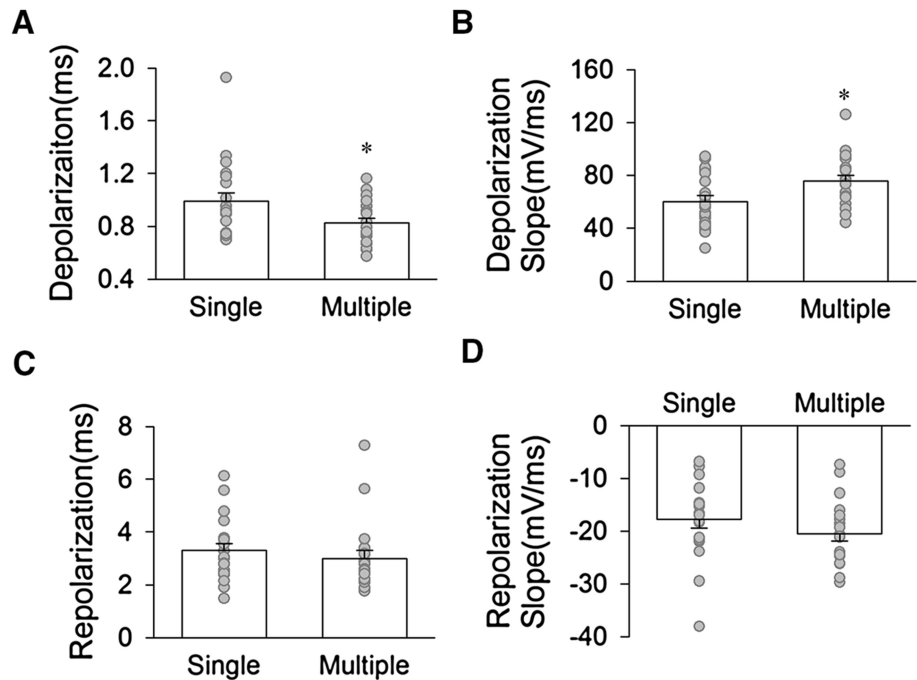
axonal component, while the second peak is considered to be a somatic component [26]. In our study, as expected, there were two divided peaks in the d^2V/dt^2 waveforms of 80.52% of action potentials in single-axon neurons, while this ratio was 59.09% in multiple-axon neurons (Fig. 6D). Interestingly, we found that 36.36% of the action potentials in multiple-axon neurons had three peaks in d^2V/dt^2 waveforms, while only 7.79% in single-axon neurons had three peaks (Fig. 6B and D). The percentage of multiple-axon neurons with three components in the rising phase was significantly higher than that of single-AIS neurons, revealing that the axon number of neurons affect their depolarization properties. According to previous reports, the first d^2V/dt^2 peak is the axonal component [26], which triggers action potential initiation, but the components of the last two peaks require further study. A waveform of d^2V/dt^2 with three components has not been reported before. In our results, there were more neurons with multiple AISs having three d^2V/dt^2 peaks than single-AIS neurons. We hypothesized that the second peak is an extra AIS component, whereas the last peak is the somatic component.

To test the hypothesis proposed above, we calculated the time interval between each two d^2V/dt^2 peaks, which represents the difference in Nav channel recruitment time between different components. The latency between the first inflection point and first peak is the time required for Nav channel recruitment at primary AIS (the AIS with a lower activation threshold in multiple-axon neurons), which is represented by T1 (Fig. 6B, right panel). T2 is the latency for AIS depolarization propagating to the

second component irrespective of whether the d^2V/dt^2 waveform contains two or three peaks. T3 is the latency from the second to the third component in d^2V/dt^2 waveforms with three peaks. The single-axon and multiple-axon neurons showed no difference in T1 or T3 (Fig. 6E). However, T2 and T1 + T2 were much shorter in multiple-axon neurons than in single-axon neurons, indicating that the first component recruits the second component faster in multiple-axon neurons (Fig. 6E). To clarify the last component, we compared its recruitment time in the single-axon and multiple-axon groups. T2 + T3 is the latency from the AIS component (primary AIS for multiple-axon neurons) to the last component, whereas T1 + T2 + T3 is the latency from action potential initiation to the last component; neither T2 + T3 nor T1 + T2 + T3 differed between the two groups (Fig. 6E). Therefore, multiple-axon neurons have a more rapidly-recruited component before the last component.

To further clarify the component of the extra peak in d^2V/dt^2, we referred to previous studies demonstrating that a higher level of Nav channels on AISs leads to a higher first peak value of d^2V/dt^2 [28, 29]. Since the AISs of living neurons were labeled by neurofascin antibodies rather than pan-Nav antibodies, we first analyzed the correlation between neurofascin and pan-Nav fluorescence intensity on each AIS using co-immunofluorescence (Figs. 2A, 6F). The results showed that the fluorescence intensity of pan-Nav on each AIS was positively correlated with that of neurofascin. Then the live-labeling fluorescence intensity of neurofascin on the AIS of single-axon neurons was compared with their first peak value of d^2V/dt^2, showing a
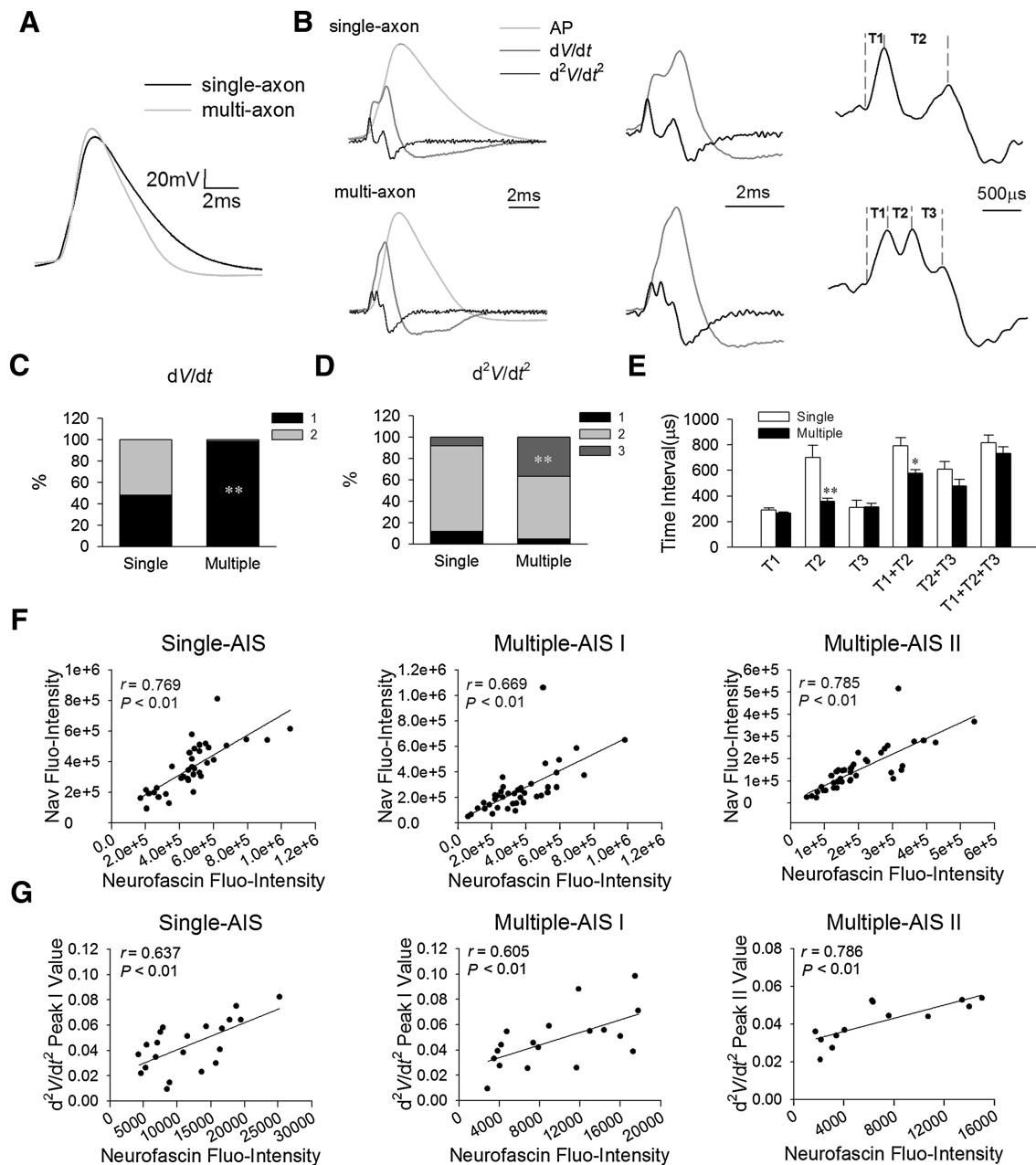
Fig. 6 The extra AISs of multiple-axon neurons accelerate action potential depolarization and fire before somatic components. **A** Typical examples of action potentials showing that the multiple-axon neuron depolarizes faster than the single-axon neuron. **B** First derivative (dV/dt, *dark grey*) and second derivative (d^2V/dt^2, *black*) from single-axon neurons (*upper panels*) and multiple-axon neurons (*lower panels*). T1 is the latency between the inflection point and the first peak; it approximates the time for primary AIS (the AIS with a lower activation threshold in multiple-axon neurons) invasion. T2 is the latency between the first and second peaks. T3 is the latency between the second and third peaks; it is the propagation time between the other two populations of channels after primary AIS depolarization. **C** The dV/dt waveforms of action potentials from multiple-axon neurons tended to fuse as one peak, while half of the single-axon neurons had 2 distinct peaks. **D** The action potentials of

multiple-AIS neurons had more 3-peak d^2V/dt^2 waveforms than those of single-axon neurons. 1, 2, and 3 indicate the number of derivative waveform peaks. (Single, $n = 77$ action potentials from 29 neurons; multiple, $n = 66$ action potentials from 20 neurons; **$P < 0.01$, proportion test). **E** The action potentials of multiple-axon neurons had a shorter time interval (T2) from primary AIS depolarization to the second part of channel recruitment (*$P < 0.05$, **$P < 0.01$, t-test). **F** Correlation between fluorescence intensity of Nav and neurofascin (single AIS, $n = 36$; multiple AIS I (the AIS with a higher level of neurofascin fluorescence), $n = 40$; multiple AIS II (the other AIS with lower level of neurofascin fluorescence in neurons with two axons), $n = 40$, from 2 experiments. **G** Correlation between fluorescence intensity of neurofascin and first/second peak values of d^2V/dt^2 with 3 peaks (single AIS, $n = 21$; multiple AIS I, $n = 18$; multiple AIS II, $n = 13$, from 2 experiments; Pearson correlation analysis).

significant correlation between the two factors (Fig. 6G, left). A similar correlation existed between neurofascin fluorescence on AIS I (the AIS with a higher level of neurofascin fluorescence) and their first peak value of d^2V/dt^2 (Fig. 6G, middle). There was a correlation between neurofascin fluorescence on AIS II (the other AIS with lower level of neurofascin fluorescence in neurons with two axons) and their second peak value among the three peaks of d^2V/dt^2 (Fig. 6G, right). Considered with the result that the density of somatic Nav channels was similar in the single- and multiple-axon neurons (Fig. 2G), these results indicated that the last component is contributed by the soma in both groups, whereas the second peak before the somatic component is the AIS II or secondary AIS (the AIS with a higher activation threshold in multiple-axon neurons) component in multiple-AIS neurons. These results revealed that supernumerary axons are electrophysiologically functional, can fire before the soma, and contribute to faster depolarization in multiple-axon neurons.

Discussion

The PI3K-Akt-GSK-3β axonal growth regulation pathway has a long history of study in the context of axon regeneration. Generating new axons by GSK-3 inhibition may help to rebuild neuronal network activity after axon injury [4]. However, the capacity of supernumerary axons induced by pharmacological treatment to function in a normal manner has not been determined.

We used SB41 to induce multiple axons, although the proportion was not as high as previously reported [4]. We attribute this to different labeling methods (Tau-1 versus AnkG). Tau-1 is a microtubule-stabilizing protein that is enriched at the distal axon and indicates the polarized structure of the axon [30, 31]. Recruitment of AnkG and ion channels at the AIS means that the axon is electrically active and can initiate action potentials [9]. We observed Nav enrichment on multiple AISs, but, surprisingly, major spiking properties were not influenced by this structural change, indicating that multiple-axon neurons have normal action potential initiation. The multiple sites of Nav channel enrichment in multiple-axon neurons were not due to up-regulation of Nav channel proteins, as indicated by the unchanged whole-cell Nav current. This indicated that the expression level of Nav channels is relatively stable, in accordance with the similar action potential amplitude in the two groups. The Nav channel fluorescence density of multiple-AIS neurons was lower than that of single-AIS neurons. However, the presence of multiple AISs shortened the rising phase of the action potential because Nav channels were recruited faster on the extra AIS.

According to previous reports, the depolarization kinetics of the action potential are determined by how the initial depolarization at the AIS region recruits Nav channels in other regions such as the soma-dendrites and the distal axon [32–34]. During patch-clamp recording, when a neuron is somatically injected with a depolarizing current, the dense Nav channels at the distal AIS region ($\sim$30–40 μm from the soma) [35, 36] are thought to open first, which determines the action potential threshold. Next, nearby Nav channels in other parts of the AIS region are recruited to form the axonal spike. Axonal depolarization further recruits somatic Nav channels which are present at a density insufficient to allow them to fire before the axonal spike [13], leading to the somatic spike.

The first derivative (dV/dt) and second derivative (d^2V/dt^2) of the action potential are powerful tools that allow assessment of action potential components. A typical dV/dt waveform has one or two peaks, and the AIS component can always be identified as a 'kink' [32]. In our experiments, almost all multiple-axon neurons had only one dV/dt peak, in which the AIS Nav channel component and soma-dendritic component were indistinguishable. This finding explains why the action potential of multiple-axon neurons depolarized faster than single-axon neurons: Nav channels were recruited faster once the AIS depolarized. The time interval between the two peaks is influenced by the distance between the AIS and the soma. When the AIS moves distally, the time interval becomes longer [27]. Therefore, the one-peak dV/dt waveform of the multiple-axon neurons is consistent with a shorter distance between the AIS and soma (Fig. 2C). The d^2V/dt^2 waveform is usually considered to have two peaks, which represent the AIS spike and the soma-dendritic spike. The time delay between the two peaks is used to calculate the propagation time from the AIS to the soma [37]. In this study, the d^2V/dt^2 waveforms of a few single-axon neurons and many multiple-axon neurons had three peaks; this finding, which has not been reported before, indicates a three-part Nav channel distribution, which corresponds well with the results of our Nav channel immunofluorescence experiments. The presence of a few single-axon neurons with d^2V/dt^2 waveforms with three peaks was attributed to the limited sensitivity of AIS live labeling. Some AISs are of insufficient size to be observed using live labeling, because the tested neurons are alive and material recycling is ongoing. Why did a few neurons with single- or multiple-axons show only one peak in d^2V/dt^2, and a majority of multiple-axon neurons show two peaks in d^2V/dt^2? The most important reason is the heterogeneity of electrophysiological properties of neurons [32]. The waveform of dV/dt or d^2V/dt^2 depends on the electrophysiological properties of each component of the neuron and the distances between them. If the distances are small enough, or the electrophysiological

properties of one AIS are similar to that of another AIS or the soma, the recruitment time would be too short to separate different components [38, 39].

Axon injury often causes permanent neurological impairment in the mature CNS. Although studies on axon regeneration have made significant progress toward understanding the underlying mechanisms, therapeutic effects have been very limited [3]. Among all the methods of inducing axon regeneration, transforming pre-existing dendrites into multiple axons has advantages over others. In this study, we examined the electrophysiological functions of SB41-induced multiple-axon hippocampal neurons. Immunostaining of AnkG, neurofascin and Nav channels indicated that the supernumerary axons of multiple-axon neurons had functional AISs. The presence of multiple axons did not change membrane properties or the action potential threshold, half-width, or amplitude. However, multiple-axon neurons depolarized faster than single-axon neurons. Analysis of the kinetics of the rising phase of the action potential revealed that the extra AIS played a role in action potential initiation by firing between the primary AIS component and soma component. These results suggest that the AIS structure of the extra axons is relatively intact and can initiate action potentials before the recruitment of soma-dendritic components. Thus, the induction of multiple AISs may provide a method for reconstructing the functional axon substructure following axon injury.

Compliance with Ethical Standards

Conflict of interest All authors declare no actual or potential conflicts of interest including any financial, personal or other relationships with other people or organizations within three years of beginning the work submitted that could inappropriately influence (bias) their work.

References

1. Barnes AP, Polleux F. Establishment of axon-dendrite polarity in developing neurons. Annu Rev Neurosci 2009, 32: 347–381.
2. Cheng PL, Poo MM. Early events in axon/dendrite polarization. Annu Rev Neurosci 2012, 35: 181–201.
3. He Z, Jin Y. Intrinsic control of axon regeneration. Neuron 2016, 90: 437–451.
4. Jiang H, Guo W, Liang X, Rao Y. Both the establishment and the maintenance of neuronal polarity require active mechanisms: critical roles of GSK-3beta and its upstream regulators. Cell 2005, 120: 123–135.

5. Yoshimura T, Kawano Y, Arimura N, Kawabata S, Kikuchi A, Kaibuchi K. GSK-3beta regulates phosphorylation of CRMP-2 and neuronal polarity. Cell 2005, 120: 137–149.
6. Witte H, Neukirchen D, Bradke F. Microtubule stabilization specifies initial neuronal polarization. J Cell Biol 2008, 180: 619–632.
7. Nakada C, Ritchie K, Oba Y, Nakamura M, Hotta Y, Iino R, *et al.* Accumulation of anchored proteins forms membrane diffusion barriers during neuronal polarization. Nat Cell Biol 2003, 5: 626–632.
8. Winckler B, Forscher P, Mellman I. A diffusion barrier maintains distribution of membrane proteins in polarized neurons. Nature 1999, 397: 698–701.
9. Kole MH, Stuart GJ. Signal processing in the axon initial segment. Neuron 2012, 73: 235–247.
10. Rasband MN. The axon initial segment and the maintenance of neuronal polarity. Nat Rev Neurosci 2010, 11: 552–562.
11. Bender KJ, Trussell LO. The physiology of the axon initial segment. Annu Rev Neurosci 2012, 35: 249–265.
12. Song AH, Wang D, Chen G, Li Y, Luo J, Duan S, *et al.* A selective filter for cytoplasmic transport at the axon initial segment. Cell 2009, 136: 1148–1160.
13. Kole MH, Ilschner SU, Kampa BM, Williams SR, Ruben PC, Stuart GJ. Action potential generation requires a high sodium channel density in the axon initial segment. Nat Neurosci 2008, 11: 178–186.
14. Nishimura K, Akiyama H, Komada M, Kamiguchi H. betaIV-spectrin forms a diffusion barrier against L1CAM at the axon initial segment. Mol Cell Neurosci 2007, 34: 422–430.
15. Lorincz A, Nusser Z. Cell-type-dependent molecular composition of the axon initial segment. J Neurosci 2008, 28: 14329–14340.
16. Jenkins SM, Bennett V. Ankyrin-G coordinates assembly of the spectrin-based membrane skeleton, voltage-gated sodium channels, and L1 CAMs at Purkinje neuron initial segments. J Cell Biol 2001, 155: 739–746.
17. Goldberg EM, Clark BD, Zagha E, Nahmani M, Erisir A, Rudy B. K+ channels at the axon initial segment dampen near-threshold excitability of neocortical fast-spiking GABAergic interneurons. Neuron 2008, 58: 387–400.
18. Hu W, Tian C, Li T, Yang M, Hou H, Shu Y. Distinct contributions of Na(v)1.6 and Na(v)1.2 in action potential initiation and backpropagation. Nat Neurosci 2009, 12: 996–1002.
19. Grubb MS, Burrone J. Activity-dependent relocation of the axon initial segment fine-tunes neuronal excitability. Nature 2010, 465: 1070–1074.
20. Sun X, Wu Y, Gu M, Liu Z, Ma Y, Li J, *et al.* Selective filtering defect at the axon initial segment in Alzheimer's disease mouse models. Proc Natl Acad Sci U S A 2014, 111: 14271–14276.
21. Schafer DP, Jha S, Liu F, Akella T, McCullough LD, Rasband MN. Disruption of the axon initial segment cytoskeleton is a new mechanism for neuronal injury. J Neurosci 2009, 29: 13242–13254.
22. Hinman JD, Rasband MN, Carmichael ST. Remodeling of the axon initial segment after focal cortical and white matter stroke. Stroke 2013, 44: 182–189.
23. Bradke F, Dotti CG. Differentiated neurons retain the capacity to generate axons from dendrites. Curr Biol 2000, 10: 1467–1470.
24. Naundorf B, Wolf F, Volgushev M. Unique features of action potential initiation in cortical neurons. Nature 2006, 440: 1060–1063.
25. Evans MD, Dumitrescu AS, Kruijssen DL, Taylor SE, Grubb MS. Rapid modulation of axon initial segment length influences repetitive spike firing. Cell Rep 2015, 13: 1233–1245.

26. Meeks JP, Mennerick S. Action potential initiation and propa-gation in CA3 pyramidal axons. J Neurophysiol 2007, 97: 3460–3472.

27. Wefelmeyer W, Cattaert D, Burrone J. Activity-dependent mismatch between axo-axonic synapses and the axon initial segment controls neuronal output. Proc Natl Acad Sci U S A 2015, 112: 9757–9762.

28. Wimmer VC, Reid CA, Mitchell S, Richards KL, Scaf BB, Leaw BT, et al. Axon initial segment dysfunction in a mouse model of genetic epilepsy with febrile seizures plus. J Clin Invest 2010, 120: 2661–2671.

29. Royeck M, Horstmann MT, Remy S, Reitze M, Yaari Y, Beck H. Role of axonal NaV1.6 sodium channels in action potential initiation of CA1 pyramidal neurons. J Neurophysiol 2008, 100: 2361–2380.

30. Kosik KS, Finch EA. MAP2 and tau segregate into dendritic and axonal domains after the elaboration of morphologically distinct neurites: an immunocytochemical study of cultured rat cerebrum. J Neurosci 1987, 7: 3142–3153.

31. Yamamoto H, Demura T, Morita M, Banker GA, Tanii T, Nakamura S. Differential neurite outgrowth is required for axon specification by cultured hippocampal neurons. J Neurochem 2012, 123: 904–910.

32. Bean BP. The action potential in mammalian central neurons. Nat Rev Neurosci 2007, 8: 451–465.

33. Williams SR, Stuart GJ. Action potential backpropagation and somato-dendritic distribution of ion channels in thalamocortical neurons. J Neurosci 2000, 20: 1307–1317.

34. Khaliq ZM, Raman IM. Relative contributions of axonal and somatic Na channels to action potential initiation in cerebellar Purkinje neurons. J Neurosci 2006, 26: 1935–1944.

35. Colbert CM, Pan E. Ion channel properties underlying axonal action potential initiation in pyramidal neurons. Nat Neurosci 2002, 5: 533–538.

36. Kress GJ, Dowling MJ, Eisenman LN, Mennerick S. Axonal sodium channel distribution shapes the depolarized action potential threshold of dentate granule neurons. Hippocampus 2010, 20: 558–571.

37. Hedrich UB, Liautard C, Kirschenbaum D, Pofahl M, Lavigne J, Liu Y, et al. Impaired action potential initiation in GABAergic interneurons causes hyperexcitable networks in an epileptic mouse model carrying a human Na(V)1.1 mutation. J Neurosci 2014, 34: 14874–14889.

38. Atherton JF, Wokosin DL, Ramanathan S, Bevan MD. Auton-omous initiation and propagation of action potentials in neurons of the subthalamic nucleus. J Physiol 2008, 586: 5679–5700.

39. Kress GJ, Dowling MJ, Meeks JP, Mennerick S. High threshold, proximal initiation, and slow conduction velocity of action potentials in dentate granule neuron mossy fibers. J Neurophysiol 2008, 100: 281–291.